ChemPubSoc Europe

DOI: 10.1002/ejic.201700241

EurJIC European Journal of Inorganic Chemistry

Full Paper

Mechanism of Reduction by Ascorbate

Redox Equilibration Observed for the Reduction of a Ruthenium(III) Complex by Ascorbate under Low-Driving-Force Conditions

Olga Impert,*[a] Anna Katafias,*[a] Marta Chrzanowska,[a] Tadeusz Muzioł,[a] Grzegorz Wrzeszcz,[a] and Rudi van Eldik*[a,b,c]

Abstract: A detailed kinetic study of the reduction of *trans*-$[RuCl_2(dipicOEt)_2]^-$, where dipicOEt = dipicolinate mono ethyl ester anion, by L-ascorbic acid that leads to the formation of the corresponding Ru^{II} complex, was carried out spectrophotometrically using the stopped-flow technique. The reaction was studied as a function of $[AscH_2]_T$ and pH. The observed kinetic traces could only be fitted by a three-exponential function, characteristic of three parallel reaction paths. The complex was isolated as $\{[Na(H_2O)_2][trans\text{-}RuCl_2(dipicOEt)_2]\}_n$, of which a single-crystal X-ray diffraction structure was determined. Detailed spectroscopic studies on the complex in aqueous solution showed that, under the selected experimental conditions, only a single complex species is present in solution. The observed complication is suggested to arise from the low driving force of the reaction during which the reoxidation of Ru^{II} by the semi-oxidized L-ascorbic acid, that is, ascorbyl radical $Asc^{\bullet-}$, accounts for the apparent three-exponential behavior of the reaction. The results are in excellent agreement with those of a recent study on the same reaction for *cis*-dichloridobispicolinatoruthenate(III) (*Eur. J. Inorg. Chem.* **2016**, 5380–5386).

Introduction

In a recent paper from our group,[1] we reported mechanistic findings for the reduction of *cis*-$[Ru^{III}Cl_2(pic)_2]^-$, where pic = picolinate anion, by ascorbic acid and found kinetic traces that were typical for three parallel reactions, independent of the selected pH. Furthermore, at lower pH and ascorbic acid concentrations, the kinetic data and overall conversion to Ru^{II} clearly showed evidence for a reversible reaction for all three reactions paths. At higher pH, no evidence of reversible reactions was found and the observed saturation kinetics were typical of an outer-sphere electron-transfer process. In an earlier study,[2] we demonstrated that the Ru^{III} compounds used in the latter study were absolutely pure and no evidence for any other species in solution was found that could account for the apparent three-parallel-reaction behavior. It was concluded, from a detailed investigation, that the observed behavior was due to redox equilibration under low-driving-force conditions that involved a back reaction of the ascorbyl radical anion with Ru^{II} to re-form the Ru^{III} complex.[1]

[a] *Faculty of Chemistry, N. Copernicus University, 87-100 Toruń, Poland*
E-mail: oimpert@umk.pl
katafias@umk.pl
web.chem.umk.pl/KChNiK
[b] *Department of Chemistry and Pharmacy, University of Erlangen-Nuremberg, 91058 Erlangen, Germany*
E-mail: rudi.vaneldik@fau.de
www.chemie.uni-erlangen.de/vaneldik
[c] *Faculty of Chemistry, Jagiellonian University, 30-033 Kraków, Poland*

Supporting information and ORCID(s) from the author(s) for this article are available on the WWW under https://doi.org/10.1002/ejic.201700241.

Notably, at that time, there was no evidence reported in the literature of the reoxidation of Ru^{II} to Ru^{III} by the ascorbyl anion radical. The reoxidation of Ru^{II} by dehydroascorbic acid (DHA) was found to occur under selected reaction conditions, but only orders of magnitude slower than the observed effect. As far as we know, there is only one report in the literature[3] where dehydroascorbic acid oxidized nitrosyl-hemoglobin to metmyoglobin and NO, and was thereby reduced to ascorbic acid.

In a parallel study, we have now found very similar behavior for a related complex, $\{[Na(H_2O)_2][trans\text{-}RuCl_2(dipicOEt)_2]\}_n$, where dipicOEt presents the dipicolinate mono ethyl ester anion, that was formed in situ during the synthesis of the complex using dipicolinate in ethanol solution. We determined the crystal structure and EPR spectrum of the isolated complex, and used spectroscopic and electrochemical techniques to characterize the nature of the complex in aqueous solution. From these studies, it is clear that only one complex ion exists in the solid state and in solution. Detailed kinetic studies of the reduction of the complex by ascorbic acid, as a function of pH and ascorbic acid concentration, were performed. The results are in excellent agreement with our earlier findings,[1] and they demonstrate, in general, the importance of back reactions during the reduction of such Ru^{III} complexes under low-driving-force conditions.

Results and Discussion

Our intention was to synthesize the bis(dipicolinato)Ru^{III} complex as a modification of the $[RuCl_2(picolinato)_2]^-$ complex ion studied before,[1,2] with the goal of changing the redox potential of the complex. Under the selected synthetic conditions, we

were not able to synthesize this complex, and we could only isolate a bis(dipicolinato) complex of which one carboxylate group of each dipicolinate ligand was esterified by ethanol.

Identification of the Complex in the Solid State

The $\{[Na(H_2O)_2][RuCl_2(dipicOEt)_2]\}_n$ complex crystallized in the triclinic $P\bar{1}$ space group, with two ruthenium atoms found on inversion centers and with half of the whole molecule given by the formula in the asymmetric unit (Figure 1). Hence, in the asymmetric unit, there are the Ru1 and Ru2 complex anions and a sodium ion with the O52 and O53 water molecules, which are also connected to both ruthenium ions through the O3 and O23 atoms of the dipicOEt anions.

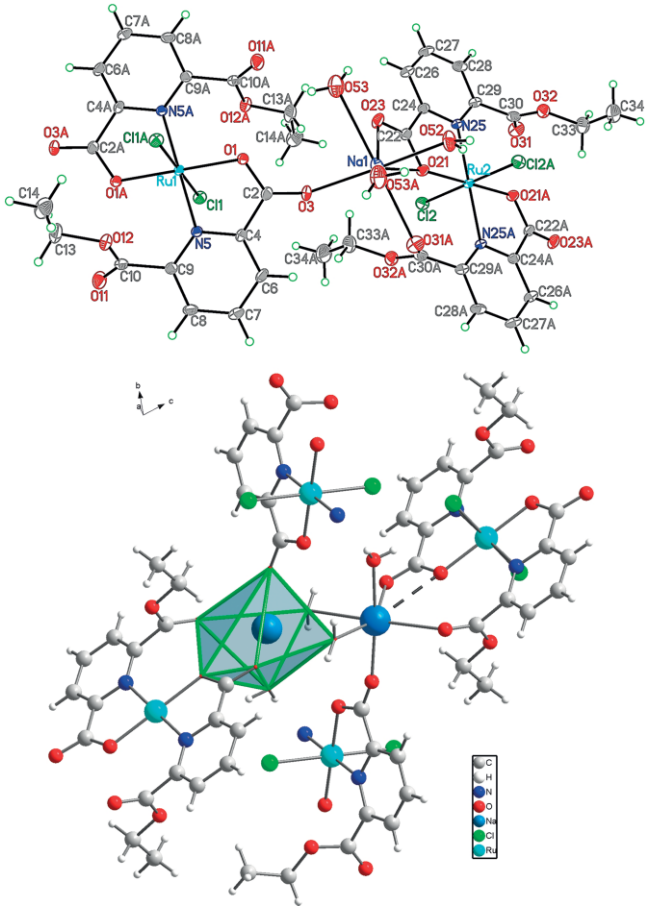

Figure 1. (a) The whole molecule given by the formula $\{[Na(H_2O)_2][trans\text{-}RuCl_2(dipicOEt)_2]\}_n$, with the numbering scheme and the thermal ellipsoids at 20 % probability. (b) Structural environment of the sodium cations forming a dimer bridged by two O53 water molecules. For one of the sodium ions, the coordination polyhedron is presented, assuming that Na1 is seven-coordinate and the O21 atom is also bound (marked by the dashed line).

The $\{[Na(H_2O)_2][RuCl_2(dipicOEt)_2]\}_n$ complex forms a three-dimensional network and the given formula is a building block of a polymer. Coordination spheres of both ruthenium centers adopt a slightly distorted octahedral environment, with the chlorido ions positioned *trans* to each other. The coordination spheres of both ruthenium centers consist of two dipicOEt moieties and two chlorido anions. Ru–Cl bond lengths are 2.3341(8) and 2.3332(9) Å for Ru1 and Ru2, respectively, whereas Ru–N and Ru–O bonds are much shorter, being 2.074(2)–2.091(2) Å and 2.015(2)–2.027(2) Å, respectively. The angles in the coordination sphere are in the range 79.58(9)–100.42(9)° and 79.99(9)–100.01(9)° for Ru1 and Ru2, respectively. Atoms positioned *trans* to each other always form an angle of 180°, due to the position of the ruthenium atoms on the inversion centers.

The coordination sphere of the sodium cation consists of six oxygen atoms, two coming from the carboxylate groups and one from the ester group of dipicOEt, as well as three from water molecules forming a facial arrangement [see Figure 1b]. The Na–O distances were found in a very wide range, from 2.302(3) to 2.815(4) Å. The sodium-ion sphere reveals a heavily tetragonally distorted octahedral environment with significant elongation of the *trans* positioned Na1–O31($-x$, $-y + 2$, $-z + 1$) and Na1–O53 bonds, being 2.724(3) and 2.815(4) Å, respectively, whereas four equatorial Na–O bond lengths were found in the range 2.302(3)–2.528(3) Å. The valence angles between atoms found in *trans* positions, of 149.65(14), 173.51(11), and 174.95(13)°, indicate additional distortion of the coordination sphere. The smallest value significantly differs from 180° and was found for O53($-x$, $-y + 2$, $-z$)–Na1–O23. In addition, semi-coordination occurs between Na1 and O21 at a distance of 2.981(3) Å, slightly longer than the sum of the van der Waals radii,[4] which can rationalize the observed deformation of the coordination sphere. Moreover, the additional coordinating atom resulted in elongation of the Na1–O23 bond to 2.528(3) Å, whereas three other equatorial distances range from 2.302(3) to 2.347(4) Å. In the coordination sphere, there are two O53 water molecules bridging adjacent sodium cations. The Na1-($-x$, $-y + 2$, $-z$)–O53–Na1 angle is 93.86(13)° and the distances to both sodium ions are very different [2.347(4) and 2.815(4) Å], revealing significant asymmetry. The O52 water molecule, involved only in hydrogen bonding, forms a short bond of 2.318(3) Å. The O3 atom of the carboxylate group, bound to Na1 in a monodentate way, forms a short bond of 2.302(3) Å, whereas the bidentate coordination mode observed for O21 in the dipicOEt anion results in significant elongation. Similarly, the O31 ester group coordinates at the long distance of 2.724(3) Å.

The structure forms a three-dimensional crystal network, due to covalent and hydrogen bonds and π–π interactions (Figure 2). However, the sodium ions play a key role in the formation of the crystal network, because they mediate interactions between ruthenium ions, due to formed covalent bridges. The packing is influenced by the positions of the metal ions, which are found close to the borders of the unit cell. The structure can be described as –Ru2–Na–Na–Ru2–Na–Na– chains, whereas the Ru1 ions are found at the centers of the (001) faces. Hence, they are positioned between adjacent chains running along the *c* axis and assure covalent connections between chains, due to bonding created by O3 atoms. In the chain, Na1 and Ru2, separated by 4.880 Å, are members of a nine-membered nonflat ring composed of Na1–O23–C22–O21–Ru2–N25–C29–C30–O31 atoms. All of these coordinating bonds assure the formation of a layer, which can be seen along the [–110] direction. These layers are connected through C26–H26···O11(x, $1 + y$, z) and C27–H27···Cl2($1 - x$, $2 - y$, $1 - z$) hydrogen bonds and π–π

interactions formed by the Ru2 chelate ring and both N5 and N25 pyridine rings.

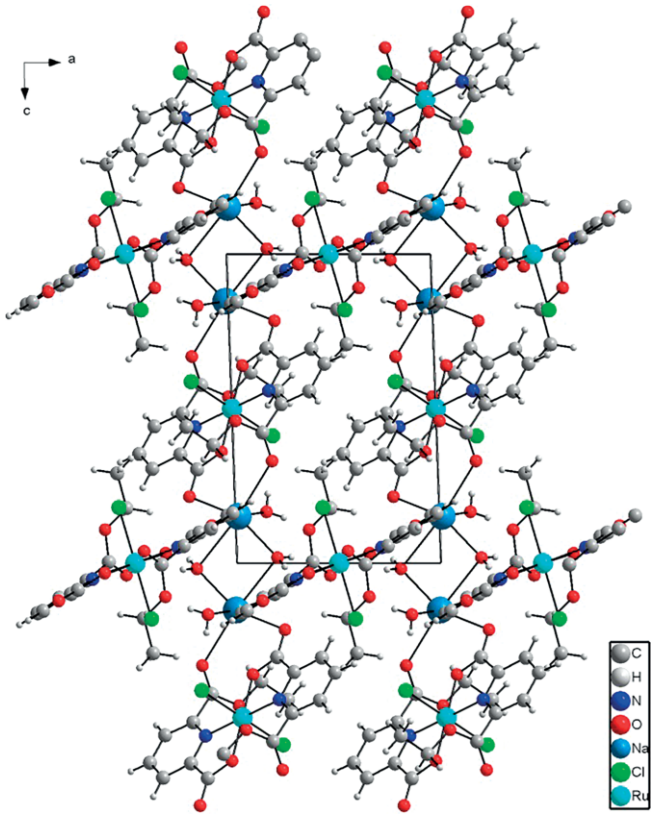

Figure 2. Packing of $\{[Na(H_2O)_2][trans\text{-}RuCl_2(dipicOEt)_2]\}_n$ along the *b* axis reveals chains of –Ru2–Na–Na–Ru2–Na–Na– running along the *c* axis and forming *bc* layers. The packing pattern shows also positions of metal ions close to the border of the unit cell.

There are few known ruthenium complexes with the dipicolinate ligand.[5–8] In all of these structures, the dipicolinate ligand was not modified, and both carboxylate groups are accessible for coordination. Hence, this ligand is usually bound in the tridentate N,O,O′ mode, with both carboxylate groups involved in the coordination. These groups are coplanar with the pyridine ring, resulting in the *mer* isomer. The *trans*-$(NH_4)[RuCl_2(dipic)_2]$ complex[9] is the only exception, because it uses only one carboxylate group and dipicolinate is bidentately coordinated, whereas the second one is strongly tilted, as was also observed for the reported structure. This complex is the most similar, among the known structures, to the reported compound, because it has the same ligands in the coordination sphere, shows the same stoichiometric ratio of picolinate/chlorido anions, and the chlorido anions are in *trans* positions. The coordination mode seems to be very important, because in these two structures, the Ru–N distances are longer than Ru–O, whereas for complexes with tridentately bound dipicolinate, the situation is different, with Ru–O bond lengths ranging from 2.050 to 2.118 Å, and Ru–N bond lengths ranging from 1.975 to 1.996 Å. In addition, we observe asymmetry of the Ru–O bonds for tridentately coordinated dipicolinate anions. For bidentately bound ligands, these distances range from 2.015 to 2.027 Å and from 2.074 to 2.091 Å, respectively. Therefore, the observed change is the effect of the shortening of the Ru–O bonds and of the elongation of the Ru–N bonds. This difference can be explained by the position of the ruthenium ions, which, in the tridentate-binding mode, must approach the nitrogen atom more closely in order to interact with both carboxylate groups.

The IR spectrum of $\{[Na(H_2O)_2][trans\text{-}RuCl_2(dipicOEt)_2]\}_n$ obviously presents characteristic absorptions of the coordinated 6-(ethoxycarbonyl)picolinate anion, the metal ligand, and the lattice water. The IR spectrum is complicated, shows many bands (see Exp. Sect.), and only tentative assignments, based on the literature data, are given below.[9–11] The strong band at 1725 cm^{-1} is assigned to the carbonyl stretching vibration of the ester group in the anionic ligand.[11] The antisymmetric and symmetric stretching vibrations of the coordinated carboxylate group are observed at 1695, 1656 (as a doublet), and 1376 cm^{-1}, respectively. A large difference, above 280 cm^{-1}, between the ν_{as} and ν_s vibrations indicates, according to the structure, monodentate coordination of the carboxylic group.[9,12] The band at 1603 cm^{-1} corresponds to the pyridine-ring vibration. The increase in the value of the ring vibration (ca. 28 cm^{-1}) from the free ligand shows the coordination of the ring nitrogen to ruthenium(III). The presence of lattice water molecules can be identified by the broad bands at 3548 and 3434 cm^{-1}, arising from antisymmetric and symmetric stretching ν(OH) vibrations, respectively. The weak bands observed in the 3100–2850 cm^{-1} range can be assigned to ν(CH) vibrations of both the pyridine ring and the ethyl group.[10,11]

There are many absorption bands in the far-infrared region (see Exp. Sect.). However, the assignment of these bands to metal–ligand interactions (Ru–O, Ru–Cl, and Ru–N) by comparison of the spectra of the uncoordinated ligand and the ruthenium complex is difficult and is not given in detail for the following reasons. (i) The symmetry of the coordination sphere is C_{2h} and one can expect nine (three stretching and six bending) vibrational modes for the $\{RuCl_2O_2N_2\}$ fragment active in the IR spectra. (ii) Ru–Cl and Ru–N vibrations usually occur in the same infrared region.[13,14] Recent data from both experimental[15,16] and theoretical (DFT) studies[17] show the following order of the ruthenium-ligand IR spectroscopic vibrations, Ru–N > Ru–O > Ru–Cl, contrary, in part, to older data.[13,14] But certainly, the broad and strong band at 323 cm^{-1} can be assigned to ν(Ru–Cl).

The $\{[Na(H_2O)_2][trans\text{-}RuCl_2(dipicOEt)_2]\}_n$ complex at room temperature has an effective magnetic moment of 1.98 B.M., which is typical for a one-unpaired-electron system. The value is consistent with low-spin d^5 ruthenium(III), where the orbital degenerate $^2T_{2g}$ (O_h) ground state is split, due to low-symmetry ligand-field effects and spin-orbit coupling.

The EPR spectrum of $\{[Na(H_2O)_2][trans\text{-}RuCl_2(dipicOEt)_2]\}_n$ in the solid state (Figure 3) exhibits two distinct resonances characteristic of the $S = {}^1/_2$ spin system, with $g_\perp = 2.45$ and $g_\parallel = 1.76$. The axial nature of the spectrum indicates the asymmetry of the electronic environment around ruthenium(III). The EPR data are in accordance with the central ion being present in the distorted-octahedral ligand environment observed in the crystal structure. The EPR parameters of $\{[Na(H_2O)_2][trans\text{-}RuCl_2(dipicOEt)_2]\}_n$ are very close to those of $[H(Hpic)_2][cis$-

$RuCl_2(pic)_2]\cdot 2H_2O$,[2] contrary to *mer*-[Ru(pic)$_3$], which shows a rhombic spectrum.[18,19]

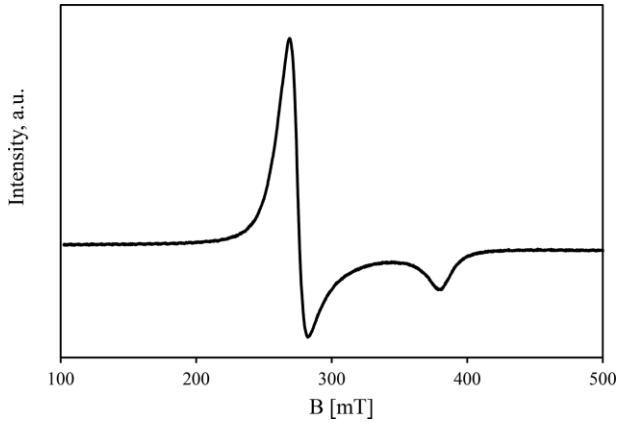

Figure 3. X-band (9.32793 GHz) EPR spectrum of powdered {[Na(H_2O)$_2$][*trans*-$RuCl_2$(dipicOEt)$_2$]}$_n$ at room temperature.

Identification of the Complex in Solution

{[Na(H_2O)$_2$][$RuCl_2$(dipicOEt)$_2$]}$_n$ is quite soluble in water. ESI-MS results demonstrate that it exists in aqueous solution as the monomeric [$RuCl_2$(dipicOEt)$_2$]$^-$ complex, m/z = 560–562, and fits the simulated spectrum (see Figure S1, Supporting Information, and Figures 4a and 4b). The multiline pattern observed in the mass spectra is due to the various isotopes centered around ^{101}Ru.

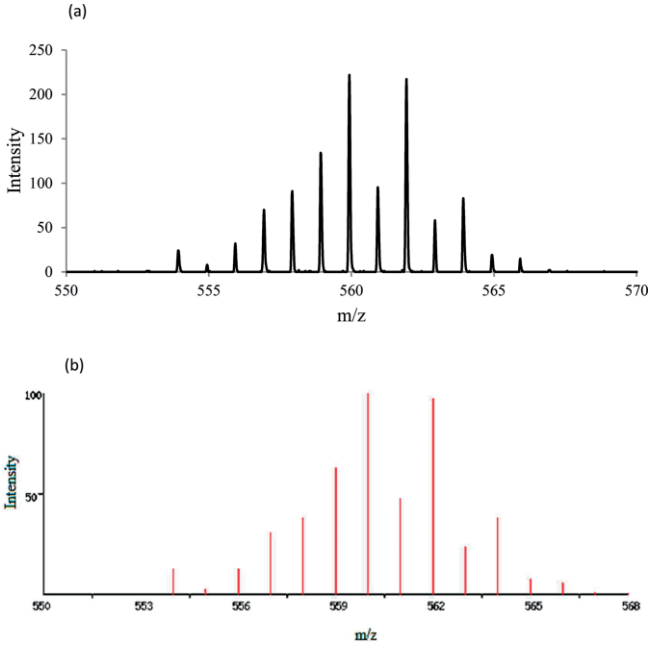

Figure 4. (a) Electrospray ionization mass spectrum of *trans*-[$RuCl_2$(dipicOEt)$_2$]$^-$ in aqueous solution; and (b) the simulated spectrum (http://www.sisweb.com/mstools/isotope.htm).

Preliminary tests have shown the expected inertness of the *trans*-[$RuCl_2$(dipicOEt)$_2$]$^-$ anion in acidic, neutral, and slightly alkaline solutions, retarding the formation of its aqua/hydroxido derivatives in spectroscopically observable concentrations. All these observations suggest that solutions obtained by dissolution of {[Na(H_2O)$_2$][*trans*-Ru $RuCl_2$(dipicOEt)$_2$]}$_n$ in water contain only one species, the *trans*-[$RuCl_2$(dipicOEt)$_2$]$^-$ complex.

The cyclic voltammogram of the examined species is presented in Figure 5. It shows a chemically quasi-reversible wave for the Ru^{III}/Ru^{II} couple; the separation of the cathodic and anodic peaks is 104 mV, and the ratio of their currents is 1.02. As expected, on the basis of the similarity to the previously studied closely related *cis*-[$RuCl_2(pic)_2]^-$ ion,[2] the *trans*-[$RuCl_2$(dipicOEt)$_2$]$^-$ complex is a very weak oxidant; values of $E_{1/2}$ for [$Ru^{III}Cl_2(pic)_2]^-$/[$Ru^{II}Cl_2(pic)_2]^{2-}$ and [$Ru^{III}Cl_2$(dipicOEt)$_2$]$^-$/[$Ru^{II}Cl_2$(dipicOEt)$_2$]$^{2-}$ are 0.030 and 0.052 V vs. SHE, respectively.

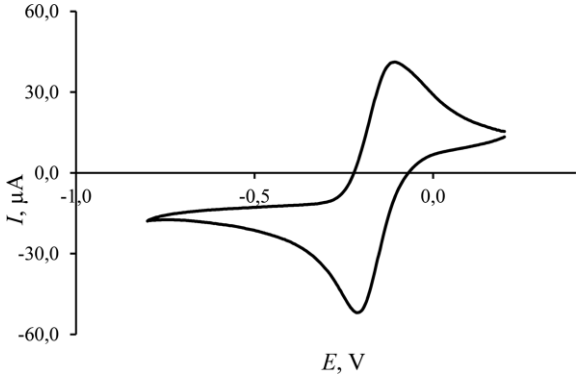

Figure 5. Cyclic voltammogram of *trans*-[$RuCl_2$(dipicOEt)$_2$]$^-$ in NaCl (0.2 M) measured vs. a silver/silver chloride, KCl (3.5 M) reference electrode, scan rate 100 mV/s.

Reduction of the Complex by Ascorbic Acid and V(II)

Although the *trans*-[$RuCl_2$(dipicOEt)$_2$]$^-$ ion is a weak oxidant, when its yellow, oxygen-free, aqueous, neutral–slightly alkaline solution is mixed with an excess of ascorbic acid (hereafter referred to as $AscH_2$) as a mild reducing agent,[20] spectral changes in the region 300–650 nm occur on a stopped-flow timescale, with a well-defined isosbestic point (at 403 nm) (Figure 6). The intense metal–ligand charge-transfer transition band formed at 549 nm evidences formation of the red ruthenium(II) species. On a much longer timescale, the observed time-dependent absorbance increase is followed by a decrease, sug-

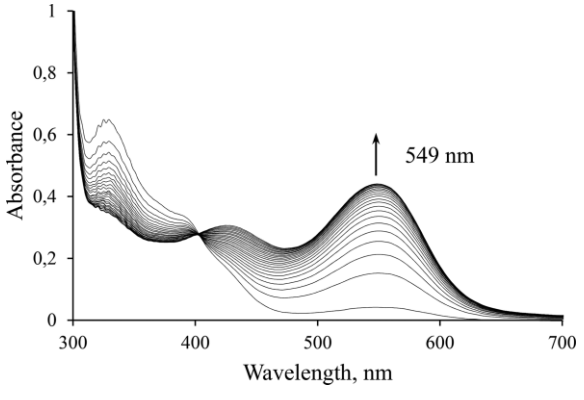

Figure 6. Typical spectral changes observed during the reaction of *trans*-[$RuCl_2$(dipicOEt)$_2$]$^-$ with ascorbate anions; [Ru^{III}] = 0.1 mM, $[AscH_2]_T$ = 1 mM, pH = 9.1, I = 0.1 M (NaCl), 25 °C, spectral scans taken every 1.2 s.

gesting hydrolysis of the resulting ruthenium(II) product. Moreover, preliminary tests, performed in the presence of air, revealed a more rapid absorbance decrease, along with a color change of the solution from red to yellow, suggesting reoxidation of ruthenium(II) by dioxygen back to ruthenium(III). To avoid any complications, the kinetics of the ruthenium(III) reduction were studied under anaerobic conditions. The stoichiometry of the redox reaction could not be determined, because of the large excess of ascorbic acid required for the reaction to go to completion under all selected experimental conditions.

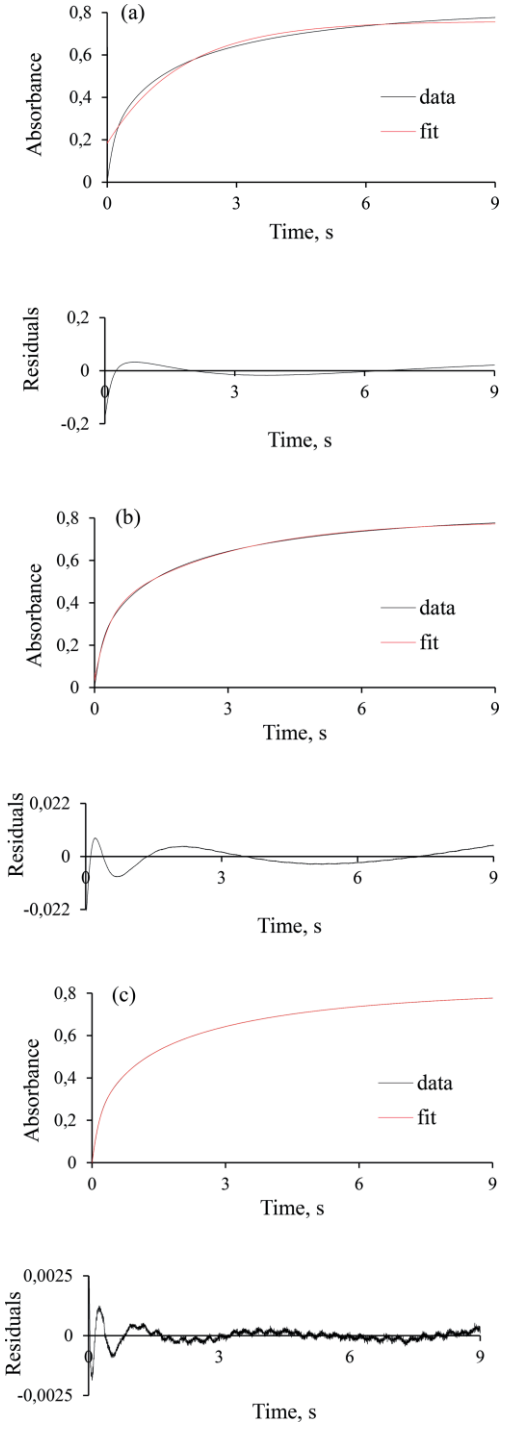

Figure 7. Typical kinetic trace recorded at 549 nm (black) for the reaction of *trans*-$[RuCl_2(dipicOEt)_2]^-$: (a) with ascorbate anions fitted to a single exponential function; (b) the sum of two exponential functions; and (c) the sum of three-exponential functions (red); $[Ru^{III}]$ = 0.1 mM, $[AscH_2]_T$ = 2 mM, pH = 9.60, I = 0.1 M (NaCl), T = 25 °C. Note the expanded scale used for the reported residuals, which clearly shows the quality of the fit.

A typical kinetic trace, recorded at the wavelength corresponding to the maximum of the ruthenium(II) absorption band, is shown in Figure 7. The absorbance increase observed under all selected reaction conditions is not at all reproduced by a single exponential function. A better fit is obtained using a sum of two exponentials, however, only the sum of three-exponential functions [Equation (1)] describes all of the kinetic time courses of the reaction in an excellent way:

$$A = A_1\exp(-k_{obs1}t) + A_2\exp(-k_{obs2}t) + A_3\exp(-k_{obs3}t) + C \quad (1)$$

This suggests that a mixture of three ruthenium(III) species of different reactivities undergoes parallel pseudo-first-order reduction reactions to give a common final product. However, as was shown above, only one reactive ruthenium(III) species exists in solution.

The kinetics of the reduction reaction were examined under pseudo-first-order conditions at varying total concentrations of the reductant (1–5 mM) and over the pH range 6.80–9.60. All of the observed rate constants, k_{obs}, measured at 549 nm and calculated using Equation (1), are reported in Table S1. Changing the wavelength had no effect on the obtained fit. We therefore analyzed the kinetic traces at the wavelength at which the largest absorbance change occurred. Notably, at a given pH, the k_{obs1}, k_{obs2}, and k_{obs3} dependencies on total ascorbic acid concentration are very similar.

Plots of k_{obs2} vs. $[AscH_2]_T$ as a function of pH are presented in Figure 8 and the corresponding profiles for k_{obs1} and k_{obs3} are given in Figure S2.

At lower pH (in the 6.80 to 8.33 range), all of the plots of k_{obs} vs. $[AscH_2]_T$ were found to be linear, with a significant intercept [Equation (2)]:

$$k_{obs} = k_a + k_b[AscH_2]_T \quad (2)$$

The slope of the linear dependence (k_b) is the second-order rate constant for the reduction reaction and the meaningful intercepts (k_a) suggest either a parallel aquation of the starting *trans*-$[RuCl_2(dipicOEt)_2]^-$ complex or a back reoxidation of the ruthenium(II) product. The values of k_a and k_b are given in Table 1.

Although no spectroscopic evidence for spontaneous aquation of the ruthenium(III) complex under the selected reaction conditions was found (vide supra), a series of kinetic measurements of the reduction reaction as a function of chlorido ion concentration within the range 0–172 mM was performed. The results collected in Table S2 clearly demonstrate that values of k_{obs1}, k_{obs2}, and k_{obs3} are practically not affected by the presence of different concentrations of chloride, thus lacking any kinetic evidence for a contribution of hydrolysis of the starting complex towards the observed intercepts. Hence, a back reaction can only account for the nonzero values of k_a [Equation (2)]. Reversibility of the studied process is supported by the effect of the total ascorbic acid concentration on the degree

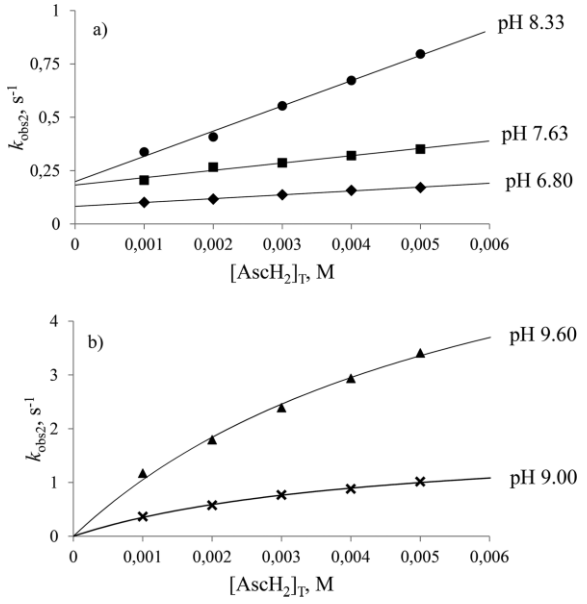

Figure 8. Total ascorbic acid-concentration dependence of the pseudo-first-order rate constant, k_{obs2}, for the second (major) phase of the reduction of *trans*-$[RuCl_2(dipicOEt)_2]^-$ by ascorbate. Experimental conditions: (a) pH = 6.80–8.33; and (b) pH = 9.00 and 9.60; I = 0.1 M (NaCl), T = 25 °C.

Table 1. Summary of values for k_a, k_b, k_c and k_cK for the reduction of *trans*-$[RuCl_2(dipicOEt)_2]^-$ by ascorbic acid; $[Ru^{III}]$ = 0.1 mM, I = 0.1 M (NaCl), T = 25 °C.

pH	Reaction phase[a]	k_b or k_cK[b] [M^{-1} s^{-1}]	k_a or k_c[b] [s^{-1}]
6.80	1	39 ± 3	0.60 ± 0.01
	2	18.1 ± 0.7	0.082 ± 0.002
	3	4.1 ± 0.3	0.013 ± 0.001
7.63	1	107 ± 5	0.92 ± 0.02
	2	34 ± 4	0.18 ± 0.01
	3	8.8 ± 0.8	0.030 ± 0.003
8.33	1	480 ± 18	0.89 ± 0.06
	2	118 ± 6	0.20 ± 0.02
	3	26.3 ± 0.4	0.039 ± 0.001
9.00[b]	1	2262 ± 72	10.9 ± 0.5
	2	431 ± 21	1.9 ± 0.1
	3	88 ± 4	0.60 ± 0.05
9.60[b]	1	7178 ± 465	38 ± 3
	2	1222 ± 10	7.5 ± 0.9
	3	263 ± 14	3.0 ± 0.4

[a] Reaction phase refers to the phase of the reaction controlled by k_{obs1}, k_{obs2}, and k_{obs3}, respectively. [b] Second-order rate constant k_cK, the initial slope of the nonlinear concentration dependence, and the limiting rate constant, k_c.

of conversion. All of the kinetic traces displayed an increase in the overall absorbance change at 549 nm; that is, an increase of the ruthenium(II) concentration, with increasing $[AscH_2]_T$. A very similar effect was caused by an increase in the pH of the solution.

Since the kinetics of the examined system were followed in deaerated solutions, the ruthenium(II) product could be reoxidized by dehydroascorbic acid (DHA); that is, the fully oxidized form of ascorbic acid generated during the forward process. Indeed, kinetic experiments clearly showed (Figure S3) the reoxidation of ruthenium(II) to ruthenium(III) by a large excess of DHA, but the observed rate constants are way too low (Figure S4), compared with the intercepts obtained for the reduction process (Table 1).

In contrast, at higher pH (in the 9.00–9.60 range), all three k_{obs} values show a nonlinear dependence on the total ascorbic acid concentration (Figures 8b and S2), which is typical of an outer-sphere electron-transfer reaction for which the kinetic saturation curves pass through the origin. Moreover, analysis of the overall spectral changes revealed that, under these conditions, the concentration of the generated ruthenium(II) complex is not affected by $[AscH_2]_T$. The latter observation, along with the zero intercepts, clearly demonstrates that, at higher pH, the reaction is shifted towards ruthenium(II) formation, and there is neither spectroscopic nor kinetic evidence for the reoxidation of ruthenium(II) back to ruthenium(III).

The kinetic data obtained for the reduction process at pH 9.00 and 9.60 presented in Figures 8b and S2 nicely fit Equation (3), in which K and k_c represent the outer-sphere encounter-complex-formation constant and the rate-limiting electron-transfer first-order rate constant, respectively:

$$k_{obs} = \frac{k_C K[AscH_2]_T}{1 + K[AscH_2]_T} \quad (3)$$

The values of k_c and k_cK for all three reaction phases are listed in Table 1.

Notably, the second-order rate constants for the reduction process, under all conditions applied in this study (k_b and k_cK), increase significantly with increasing pH (Table 1). It should be kept in mind that in aqueous solution (pH 2–14), ascorbic acid can exist in three protolytic forms: $AscH_2$, $AscH^-$, and Asc^{2-}. The corresponding pK_a values are 4.1 and 11.3,[20] from which it follows that the ascorbate monoanion ($AscH^-$) is the predominant form (> 98 %) of the reductant in the overall examined pH range. The reducing abilities of the protolytic forms differ significantly from each other, viz. the fully protonated acid ($AscH_2$) is a much weaker reductant than its conjugate base ($AscH^-$), which, in turn, is much less reactive than the fully deprotonated Asc^{2-}. The corresponding redox potentials are reported in our recent paper.[1] The clear dependence of the second-order rate constants (k_b and k_cK) for all three reaction phases on the pH of the solution (Table 1) shows that the ascorbate dianion (Asc^{2-}), though present in a very low concentration (0.003 to ca. 2 % at pH 6.80–9.60), is the actual reactive electron donor.

Similar behavior, namely the apparent three-exponential absorbance vs. time profiles, reversibility of the process at lower $[AscH_2]_T$ and pH on the one hand, and lack of evidence for a back reaction and total conversion of ruthenium(III) to ruthenium(II) at higher pH on the other hand, was recently found by us for a closely related complex, *cis*-$[RuCl_2(pic)_2]^-$.[1] Hence, electron-transfer reactions in both the studied systems proceed according to the same mechanism. A typical mechanism reported in the literature for the irreversible ascorbic acid reduction of inert ruthenium(III) (or any other metal) complexes involves two consecutive outer-sphere electron-transfer steps, as outlined by Equations (4)–(6).[1]

$$AscH^- + [Ru^{III}] \xrightarrow{k_{ca}} [Ru^{II}] + Asc^{\bullet -} + H^+_{aq} \quad (4)$$

$$H^+_{aq} \rightleftharpoons K_{a_2}$$

$$Asc^{2-} + [Ru^{III}] \xrightarrow{k_{cb}} [Ru^{II}] + Asc^{\bullet -} \quad (5)$$

$$[Ru^{III}] + Asc^{\bullet -} \longrightarrow [Ru^{II}] + DHA \quad (6)$$

$$[Ru^{II}] + Asc^{\bullet -} + H^+_{aq} \longrightarrow [Ru^{III}] + AscH^- \quad (7)$$

In the rate-determining one-electron reduction steps [Equations (4) and (5)], ascorbate mono- and dianions reduce ruthenium(III) to ruthenium(II), while being oxidized to an intermediate ascorbyl radical ($Asc^{\bullet -}$). In the second kinetically indistinguishable step [Equation (6)], the radical reacts with another starting ruthenium(III) species to form the fully oxidized form of ascorbic acid, dehydroascorbic acid (its protolytic forms have been omitted for simplicity). However, complex kinetics found for the reduction of the *cis*-$[RuCl_2(pic)_2]^-$ ion could not be explained by the straightforward mechanism represented by Equations (4)–(6). Since dioxygen and DHA have been excluded as possible oxidants of the generated ruthenium(II), the mechanistic complications were ascribed to redox equilibration involving reoxidation of ruthenium(II) to ruthenium(III) by the ascorbyl radical [Equation (7)].[1] The redox equilibration arises, in turn, from the low driving force of the studied reactions. Indeed, both the ruthenium(III) complexes are very weak oxidants (characterized by a comparable redox potential, vide supra) and the ascorbate monoanion is a mild reductant. The thermodynamic driving force for the overall redox process is the oxidation of $Asc^{\bullet -}$ to DHA [Equation (6)]. Its value varies from +0.22 (pH 6.8) to +0.31 V (pH 9.6) and from +0.19 (pH 7) to +0.29 V (pH 9.7) for the *trans*-$[RuCl_2(dipicOEt)_2]^-$ and *cis*-$[RuCl_2(pic)_2]^-$ complexes, respectively. On the other hand, under the same conditions, the driving force for the reduction of $Asc^{\bullet -}$ by the corresponding ruthenium(II) complexes, Equation (7), varies from +0.26 (pH 6.8) to +0.10 V (pH 9.6) and from +0.28 (pH 7) to +0.12 V (pH 9.7), respectively. Comparison of these values shows that in the studied systems, oxidation and reduction of the ascorbyl radical by ruthenium(III) and ruthenium(II), respectively, are concurrent reactions, and as a consequence, the reduction of ruthenium(III) to ruthenium(II) is a reversible process. An increase in pH, resulting in an increase of the driving force, favors the reaction in Equation (6) and shifts the overall process towards the ruthenium(II) species, so that in more alkaline media, the back reaction is not seen anymore (Figure 8). Nevertheless, the three-exponential kinetic traces manifesting the dual role of the ascorbyl radical are found under all studied conditions.

Strong support for the proposed mechanism and role of the ascorbyl radical in low-driving-force systems was provided by the results of some kinetic tests on the reduction of *trans*-$[RuCl_2(dipicOEt)_2]^-$ by a strong reducing agent, vanadium(II).[21] If the mechanistic complications found for the ascorbate system are due to the redox equilibration involving the ascorbate radical under low-driving-force conditions, the complementary electron transfer from the very labile vanadium(II) to ruthenium(III) [Equation (8)], characterized by a much higher driving force (–0.03 to +0.05 V over the pH range 6.8 to 9.6 vs. +0.13 V at pH 3–3.5 for the ascorbate and vanadium systems, respectively), should proceed according to the straightforward inner-sphere reaction path.

$$[Ru^{III}] + V^{2+}_{aq} \rightarrow [Ru^{II}] + V(OH)^{2+}_{aq} + H^+_{aq} \quad (8)$$

Indeed, the observed spectral changes presented in Figure 9 are typical for a first-order reaction, and the absorbance vs. time profile given in Figure 10 is excellently reproduced by a single exponential function.

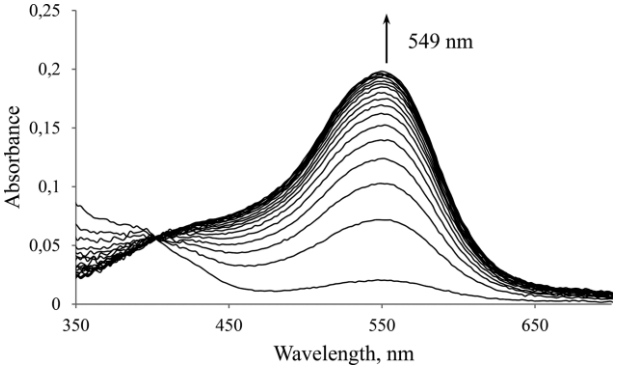

Figure 9. Typical spectral changes observed during the reduction of *trans*-$[RuCl_2(dipicOEt)_2]^-$ by V(II). Experimental conditions: $[Ru^{III}]$ = 0.02 mM, [V(II)] = 0.1 mM, pH = 4.90 (acetate buffer), I = 0.1 M ($NaClO_4$), T = 2 °C, scans taken every 5 ms.

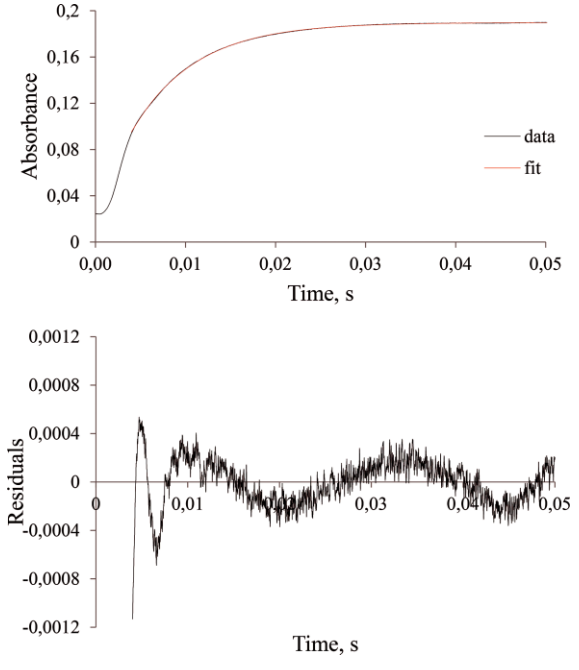

Figure 10. Typical kinetic trace recorded at 549 nm (black) for the reaction of *trans*-$[RuCl_2(dipicOEt)_2]^-$ with V(II) fitted to a single exponential (red); $[Ru^{III}]$ = 0.02 mM, [V(II)] = 0.2 mM, pH = 4.90 (acetate buffer), I = 0.1 M ($NaClO_4$), T = 2 °C. The first part of the kinetic trace is affected by the dead time of the stopped-flow instrument, which is 2–4 ms. The calculated rate constant for the reaction is (142.15 ± 0.04) s^{-1}. Note the expanded scale used for the reported residuals.

According to the above discussion, the observed increase in the reaction rate with increasing pH is a consequence of the increasing driving force of the studied process due to the de-

protonation of the ascorbate monoanion. In terms of the proposed mechanism [Equations (4)–(6)], the second-order rate constant k (Table 1) vs. $[H^+_{aq}]$ can be described by Equation (9), in which k_{ca}, k_{cb}, and K_{a2} represent the second-order rate constants for the reduction by $AscH^-$ and Asc^{2-}, and the acid-dissociation constant of $AscH^-$, respectively. This equation simplifies to Equation (10), on the assumption that $[H^+_{aq}] >> K_{a2}$.

$$k = \frac{2k_{ca}[H^+_{aq}] + 2k_{cb}K_{a2}}{K_{a2} + [H^+_{aq}]} \quad (9)$$

$$k = 2k_{ca} + \frac{2k_{cb}K_{a2}}{[H^+_{aq}]} \quad (10)$$

The corresponding fit of the kinetic data for the second phase of the *trans*-$[RuCl_2(dipicOEt)_2]^-$ transformation is presented in Figures S5 and S6. The values of k_{ca} and k_{cb}, calculated with the aid of the literature value of K_{a2}, are (25 ± 15) and (300 ± 15) × 10^2 M^{-1} s^{-1}, respectively. The relevant values found for the *cis*-$[RuCl_2(pic)_2]^-$ species were similar; that is, k_{ca} = (11 ± 2) and k_{cb} = (326 ± 2) × 10^2 M^{-1} s^{-1}. Similar reaction rates were expected for the closely related systems of comparable thermodynamic driving force studied under similar conditions (Figure 11). The higher, by three to four orders of magnitude, values for k_{cb} than those for k_{ca} confirm that Asc^{2-} is the major reductant for both investigated complexes.

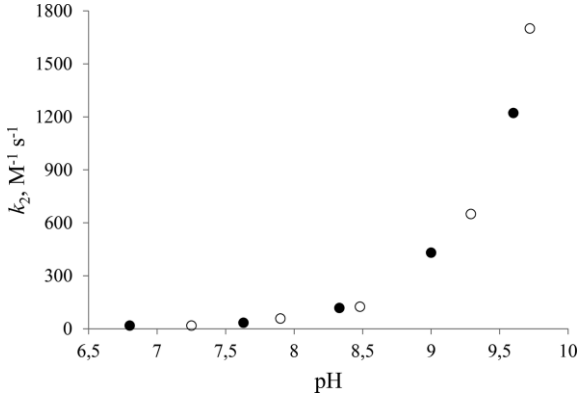

Figure 11. Dependence of the second-order rate constants for the second phase of the reaction k_2 (≡ k_b or k_cK, see Table 1) for the reduction of *trans*-$[RuCl_2(dipicOEt)_2]^-$ (●) and *cis*-$[RuCl_2(pic)_2]^-$ (○) by ascorbic acid on pH, T = 25 °C.

Conclusion

In comparison with our earlier work on the reduction of *cis*-$[RuCl_2(pic)_2]^-$ by ascorbic acid, the results of this study show that the esterification of dipicolinate during the synthesis of the corresponding dichlorido complex, *trans*-$[RuCl_2(dipicOEt)_2]^-$, had no significant influence on the kinetic data and mechanistic interpretation for the redox reaction. This is probably related to the fact that the coordination sphere of the ruthenium(II) center is very similar in both complexes. Nevertheless, the newly synthesized complex offered us the possibility to check the interpretation of our earlier work with the availability of a second system. The obtained results again point to redox equilibration causing mechanistic complications that can occur when studying low-driving-force processes. In our studies, reversible electron transfer to and from the semioxidized ascorbate, viz. the ascorbyl radical, results in the apparent three-exponential kinetics found for the ruthenium(III) reduction reaction.

Experimental Section

Materials: All chemicals were obtained from commercial sources (Sigma–Aldrich, POCh Gliwice, Poland) as pro analysis grade and were used as supplied. Deionized (Millipore) or redistilled water (from alkaline permanganate) was used to prepare all aqueous solutions.

Preparation of {[Na(H$_2$O)$_2$][*trans*-RuCl$_2$(dipicOEt)$_2$]}$_n$: Dipicolinic acid (1.67 g, 10 mmol) and NaOH (0.2 g, 5 mmol) in a minimum volume of anhydrous ethanol (ca. 5 mL) was added to a hot ethanolic solution of commercial $RuCl_3 \cdot nH_2O$ (1.007 g, 5 mmol, 30 mL), treated as previously reported.[2] The vigorously stirred mixture was refluxed for ca. 5 h. After three days, a yellow powder and few red crystals were formed. The solution was filtered, and the solid was washed three times with 5 mL of cold anhydrous ethanol and air dried. Yield 1.7 g (ca. 55 %). The red crystals were used in the single-crystal X-ray diffraction study. Both the yellow powder and the red crystals turned out to be the same compound, showing the same spectroscopic and kinetic behavior. In addition, grinding the red crystals gave a yellow powder. Elemental Anal. $C_{18}H_{20}Cl_2N_2NaO_{10}Ru$ (619.32): C 34.91, H 3.255, N 4.523; found C 34.82, H 3.550, N 5.679. UV/Visible spectrum [H_2O; λ_{max}, nm (ε, M^{-1} cm^{-1})]: 260 (13600), 329 (6000), 384 (3900). IR (KBr): 3548 (m), 3433 (m, br.), 3091 (w), 2985 (w), 2945 (w), 1725 (s), 1695 (s), 1656 (vs), 1603 (s), 1466 (m), 1444 (w), 1416 (m), 1397 (m), 1376 (s), 1341 (s), 1311 (s), 1259 (m), 1195 (sh), 1177 (s), 1115 (m), 1094 (m), 1013 (m), 932 (w), 866 (m), 838 (m), 769 (s), 750 (m), 734 (m), 674 (vw), 582 (w) cm^{-1}. FIR (PE): 554 (m), 465 (m), 395 (m), 343 (sh), 323 (s, br.), 248 (m), 192 (w), 154 (m) cm^{-1}.

Instrumentation

Elemental analysis (C, N, H) was performed with a Vario MACRON CHN analyzer, ELEMENTAR Analysensysteme GmbH. The content of ruthenium in solution was determined using a Microwave Plasma Atomic Emission Spectrometer, Agilent Technologies A100 MP-AES. Electrospray ionization mass spectrometric measurements were conducted with a Bruker MicroTOF-Q instrument in the negative-ion mode. IR spectra were recorded with a Perkin–Elmer FTIR 2000 spectrophotometer in both the 4000–400 cm^{-1} and 700–100 cm^{-1} ranges, using KBr discs and a PE (polyethylene) pellet, respectively.

Electronic absorption spectra of aqueous solutions within the UV/Vis range were recorded with a HP 8453 spectrophotometer, using quartz cuvettes, with an optical path length of 10 mm. An Elmetron CX 71 pH-meter was used to measure the pH of the solutions.

Magnetic susceptibility was measured at room temperature by the Faraday method with a balance constructed in our laboratory at a field strength of 1.0 T. The magnetic field was calibrated with $Hg[Co(NCS)_4]$.[22] The molar susceptibility was corrected for diamagnetism using Pascal's constants.[23]

The EPR spectrum of a powdered sample was recorded at room temperature with an X band (ca. 9.33 GHz) Radiopan EPR SE/X-2541M spectrometer with a 100 kHz modulation. The microwave frequency was monitored with a frequency meter. The magnetic field was measured with an automatic NMR-type magnetometer.

Cyclic voltammetry experiments were performed using a Metrohm 746 VA.TRACE ANALYZER with 747 VA STAND instrument. Glassy

carbon, platinum wire, and silver/silver chloride (3.5 M KCl) electrodes were used as the working, auxiliary, and reference electrodes, respectively. All measurements were carried out for 5 mM aqueous ruthenium(III) complex solutions with 0.2 M NaCl as the supporting electrolyte. All cyclic voltammograms were recorded under argon atmosphere at room temperature. The potential and sweep rate were changed within the 200–800 mV and 25–100 mV/s ranges, respectively. The voltammograms were independent of the scan rate. $E_{1/2}$ values were estimated as the average of the oxidative and reductive peak potentials; that is, $(E_{p,a} + E_{p,c})/2$.

X-ray Diffraction Crystallography: Diffraction data of the complex were collected with an Oxford Sapphire instrument with CCD area detector[24] for a yellow crystal of 0.25 × 0.16 × 0.04 mm dimensions. The structure was solved by direct methods and refined by full-matrix least-squares techniques on F^2 with the SHELXL program.[25,26] A numerical absorption correction was applied.[24] All heavy atoms were refined with anisotropic thermal displacement parameters. Positions of hydrogen atoms attached to carbon atoms were assigned at calculated positions and refined with isotropic thermal displacement parameters fixed to a value of 20 or 50 % higher than those of the corresponding carbon atoms. Hydrogen atoms of water molecules were found from electron-density synthesis and refined with isotropic thermal displacement parameters fixed to a value of 50 % higher than for the oxygen atom to which they were attached. For O53 water molecules, two restraints were applied (DFIX for O–H bond lengths). All figures were prepared in DIAMOND and ORTEP-3.[27,28] The results from data collections and refinement are summarized in Table 2. Selected bond lengths and bond angles are given in Table S3. CCDC 1533172 (for $\{[Na(H_2O)_2][RuCl_2(dipicOEt)_2]\}_n$) contains the supplementary crystallographic data for this paper. These data can be obtained free of charge from The Cambridge Crystallographic Data Centre.

Kinetic Measurements: Solutions of the Ru^{III} complex and ascorbic acid ($AscH_2$) were freshly prepared before use. Carbonate, TRIS and acetate buffers, and hydrochloric and perchloric acids, were used to adjust the pH of the solutions. The ionic strength was kept constant with sodium chloride or perchlorate. Further details on the selected conditions for individual experiments are given in the figure and table captions. All kinetic measurements were performed under argon atmosphere. Spectral changes and kinetic traces were recorded under pseudo-first-order conditions at 25 ± 0.1 °C, unless stated otherwise, with an Applied Photophysics SX20 stopped-flow spectrophotometer, equipped with a photodiode array detector, in addition to a single-wavelength detector. The absorbance vs. time changes were followed in the range of the Ru^{II} absorption band; that is, at 549 nm. The observed rate constants are reported as mean values of 6–8 kinetic runs and were reproducible to within ± 2 %.

Table 2. Crystal data and structure refinement.

Parameters	$\{[Na(H_2O)_2][RuCl_2(dipicOEt)_2]\}_n$
Empirical formula	$C_{18}H_{20}Cl_2N_2NaO_{10}Ru$
Formula mass [g mol^{-1}]	619.32
Temperature [°C]	20(2)
Wavelength [Å]	0.71073
Crystal system, space group	triclinic, $P\bar{1}$
Unit cell dimensions	
a [Å]	8.7740(4)
b [Å]	11.7214(8)
c [Å]	13.1054(8)
α [°]	71.441(6)
β [°]	81.675(5)
γ [°]	68.934(5)
Volume [Å^3]	1191.62(12)
Z, Calculated density [Mg m^{-3}]	2, 1.726
Absorption coefficient [mm^{-1}]	0.956
F(000)	622
Crystal size [mm]	0.25 × 0.16 × 0.04
Theta range for data collection [°]	2.15 to 26.73
Limiting indices	$-10 \le h \le 11$ $-13 \le k \le 14$ $-13 \le l \le 16$
Reflections collected/unique	7852/4984, [R(int) = 0.0407]
Completeness to theta [%]	26.73, 98.5
Absorption correction	Numerical
Max. and min. transmission	0.9628 and 0.7961
Refinement method	Full-matrix least-squares on F^2
Data/restraints/parameters	4984/2/324
Goodness-of-fit on F^2	0.833
Final R indices [$I > 2\sigma(I)$]	$R1$ = 0.0323, $wR2$ = 0.0621
R indices (all data)	$R1$ = 0.0623, $wR2$ = 0.0692
Largest diff. peak and hole [e Å^{-3}]	0.406 and −0.467

Acknowledgments

Experts at the analytical facilities of the Chemistry Institute at the University of Debrecen, Hungary, are acknowledged for their kind support. The stopped-flow measurements were performed at the Faculty of Chemistry, Jagiellonian University in Kraków, Poland.

Keywords: Redox chemistry · Kinetics · Ruthenium · Reduction · Ascorbate

[1] O. Impert, A. Katafias, J. Fenska, M. Chrzanowska, S. Koter, C. Dücker-Benfer, R. van Eldik, *Eur. J. Inorg. Chem.* **2016**, 5380–5386.
[2] O. Impert, A. Katafias, G. Wrzeszcz, T. Muzioł, K. Hrynkiewicz, N. Olejnik, M. Chrzanowska, R. van Eldik, *J. Coord. Chem.* **2016**, *69*, 2107–2120.
[3] N. Sibmooh, B. Piknova, F. Rizzatti, A. N. Schechter, *Biochemistry* **2008**, *47*, 2989–2996.
[4] A. L. Spek, *Acta Crystallogr., Sect. D: Biol. Crystallogr.* **2009**, *65*, 148–155.
[5] S. M. Couchman, J. M. Dominguez-Vera, J. C. Jeffery, C. A. McKee, S. Nevitt, M. Pohlman, C. M. White, M. D. Ward, *Polyhedron* **1998**, *17*, 3541–3550.
[6] M. K. Tse, S. Bhor, M. Klawonn, G. Anilkumar, H. Jiao, C. Dobler, A. Spannenberg, W. Magerlein, H. Hugl, M. Beller, *Chem. Eur. J.* **2006**, *12*, 1855–1874.
[7] D. Sukanya, R. Prabhakaran, K. Natarajan, *Polyhedron* **2006**, *25*, 2223–2228.
[8] D. Ventur, K. Wieghardt, J. Weiss, *Z. Anorg. Allg. Chem.* **1985**, *524*, 40–50.
[9] K. Nakamoto, *Infrared and Raman Spectra of Inorganic and Coordination Compounds*, 6th ed., Wiley, Hoboken, **2009**.
[10] Y.-F. Xie, H. Zhu, H.-T. Shi, A.-Q. Jia, Q.-F. Hang, *Inorg. Chim. Acta* **2015**, *428*, 147–153.
[11] A. M. Kirillov, M. Haukka, M. F. C. Guedes da Silva, A. J. L. Pombeiro, *Eur. J. Inorg. Chem.* **2007**, 1556–1565.
[12] G. B. Deacon, R. J. Phillips, *Coord. Chem. Rev.* **1980**, *33*, 227–250.
[13] A. E. M. Boelrijk, T. X. Neenan, J. Reedijk, *J. Chem. Soc., Dalton Trans.* **1997**, 4561–4570.
[14] R. A. Krause, K. Krause, *Inorg. Chem.* **1980**, *19*, 2600–2603.
[15] I. P. Ejidike, P. A. Ajibade, *Bioinorg. Chem. Appl.* **2016**, Article ID 9672451.
[16] I. P. Ejidike, P. A. Ajibade, *Int. J. Mol. Sci.* **2016**, *17*, 60–70.
[17] A. A. Adeniyi, P. A. Ajibade, *J. Chem.* **2016**, Article ID 3672062.
[18] N. Ghatak, J. Chakravarty, S. Bhattacharya, *Polyhedron* **1995**, *14*, 3591–3597.
[19] O. Impert, A. Katafias, P. Kita, G. Wrzeszcz, J. Fenska, G. Lente, I. Fábián, *Trans. Met. Chem.* **2011**, *36*, 761–766.

[20] A. Katafias, O. Impert, P. Kita, J. Fenska, S. Koter, A. Kaczmarek-Kędziera, H. Różycki, A. Bajek, M. Uzarska, R. van Eldik, *Eur. J. Inorg. Chem.* **2014**, 2529–2535.
[21] P. Atkins, T. Overton, J. Rourke, M. Weller, F. Armstrong, *Shriver and Atkins Inorganic Chemistry*, 5th ed., Oxford University Press, Oxford, **2010**, pp. 792, 798.
[22] N. Figgis, R. S. Nyholm, *J. Chem. Soc.* **1958**, 4190–4191.
[23] E. König, *Magnetic Properties of Coordination and Organometallic Transition Metal Compounds*, Springer-Verlag, Berlin, Heidelberg, New York, **1966**.
[24] *CrysAlis RED* and *CrysAlis CCD* **2000**, Oxford Diffraction Ltd., Abingdon, Oxfordshire, England.
[25] G. M. Sheldrick, *SHELXS97*, *SHELXL97* and *CIFTAB*, University of Göttingen, Germany, **1997**.
[26] G. M. Sheldrick, *Acta Crystallogr., Sect. A: Found. Crystallogr.* **2008**, *64*, 112–122.
[27] K. Brandenburg, *DIAMOND*, Release 2.1e, Crystal Impact GbR, Bonn, Germany, **2001**.
[28] L. J. Farrugia, *J. Appl. Crystallogr.* **1997**, *30*, 565–566.

Received: March 6, 2017

